ICEO Micropump: Electronic Supplementary Information

I. EXPERIMENTAL METHODS

A. Janus array fabrication

Fused silica substrates (500 μm DSP, University Wafer) were cleaned in 2:1 H_2SO_4:H_2O_2 at 120°C for 10'. A dehydration bake was performed in a convection oven for 30' at 160°C. SU-8 2015 was spun to a 10 μm thickness (500 rpm, 5"; 4700 rpm, 45"). A soft bake was then performed (65°C, 1'; 95°C, 3'; 65°C, 1'). Exposure was performed using a chrome mask (made using a DWL 200 maskwriter) and an MJB-3 aligner at 7.5 mW/cm^2 through a long pass filter (Omega Optical) for 2'15". A post exposure bake was then performed (65°C, 1'; 95°C, 4'; 65°C, 1'). The SU-8 was developed by dipping in SU-8 developer for 20", then rinsing in isopropanol. The substrate was then sprayed with SU-8 developer from a spray bottle, followed by isopropanol from a spray bottle, then repeating this procedure 3 additional times by alternating between SU-8 Developer and isopropanol spraying. The substrate was then inspected using a microscope, and if fully developed, a hard bake was performed at 160°C for 20'.

The liftoff resist (AZ5214) was patterned immediately after the hard bake. HMDS was spun at 2500 rpm for 30", followed by spin coating of AZ5214 resist (500 rpm, 5"; 2000 rpm, 30"). A softbake was performed at 95°C for 2'. A transparency mask (CAD/Art Services) containing the liftoff mask geometry was inserted into an MJB-3 aligner. The substrate was aligned and exposed at 7.5 mW/cm^2 for 12". The substrate was then baked at 110°C for 1', followed by a UV flood expose for 1'. The substrate was then developed for 5' using AZ726MIF developer and rinsed in DI water. The resulting photoresist liftoff mask contained a rectangular gap within the SU-8 array, as well as gaps defining the driving electrode geometry (2 cm x 300 μm electrodes connected to 5mmx5mm pads).

Just prior to performing the metal evaporation, a brief O_2 plasma clean was again performed (Technics PEIIA, 100 W/300 mTorr O_2, 2'). The electron beam evaporator (Sharon 4-pocket, single sample chamber, UCSB Nanofabrication Facility) was then loaded with the sample by setting the sample holder to a 40-42° angle with the vertical axis. The chamber was pumped to below 3x10^{-6} Torr and two evaporation steps were performed (5 nm Ti/50 nm Au, .05/.2 nm/s, no sample rotation). A gentle solvent liftoff was then performed. First, the photoresist was removed by spraying with an acetone spray bottle. The substrate was then rinsed with isopropanol. The substrate was then briefly sonicated on the lowest power setting for 10" in acetone; the sonication had to be brief and gentle to avoid SU-8 liftoff, but was necessary to liftoff the resist between the driving electrodes and array. The substrate was then rinsed with acetone again for approximately 20" while gently agitating, followed by isopropanol again for 20" under gentle agitation. The final acetone/isopropanol rinse under gentle agitation was repeated 2 additional times.

B. Multilayer PDMS device fabrication

Multilayer PDMS molds were fabricated using standard Multilayer Soft Lithography (MSL) procedures for "push-up" valves [1] and the geometry shown in the main text. Briefly, two separate molds were fabricated. The first (bottom layer) mold contained two photoresist coatings. A 10 μm SU-8 2015 layer was coated using the same procedure as above to define the pump and loop channel. An 18 μm layer of SU-8 2015 was patterned after this at 2000 rpm to define the 150 μm wide control channels for MSL valves. The second mold contained the 150 μm wide curved channels (top,"flow layer" or "injection layer"), which were patterned using a double coat of SPR 220-7. (1750 rpm for 45", bake at 110°C for 90", repeat the coating and bake, expose for 70", and develop for 5-10' until fully developed in 2:1 water:AZ400K) A reflow at 190°C for 2 hr resulted in 25 μm tall curved channels. The wafers were then treated with a non-stick fluorosilane vapors ((tridecafluoro-11,22-tetrahydrooctyl)-trichlorosilane, Gelest Inc, 20' in vacuum dessicator). The remaining details of the multilayer PDMS device fabrication may be found in the MSL literature, while the remaining device fabrication steps are found in the main text.

C. Electrolyte preparation and conductivities

Strong electrolytes (KCl and NaCl) were prepared at 100 μM concentrations. Weak electrolytes (all others) were prepared by adding 100 μM of the acid or base (chloroacetic acid, acetic acid, MES, MOPS, or Tris) to 100 μM of the sodium or chloride conjugate (sodium chloroacetate, sodium acetate, MES sodium salt, MOPS sodium salt, or Tris-HCl, respectively). The table below gives several relevant properties of each solution. The solution pK_a's are from literature [2]. The ionic strength of the weak electrolyte solutions was calculated from the equilibrium concentration of sodium, hydronium, and conjugate base, which were determined from the initial concentrations and pK_a. The electrical conductivity of each solution was measured using an Oakton ECTestr11+ conductivity meter.

Electrolyte	pK_a	Ionic strength (μM)	Conductivity (μS/cm)
KCl	-	100	28.6
NaCl	-	100	24.5
Chloroacetate	2.9	190	21.4
Acetate	4.8	110	19.6
MES	6.2	100	14.8
MOPS	7.2	100	12.8
Tris	8.3	100	17.9

II. PRESSURE AND FLOW RATE DERIVATION

The calculation for maximum pressure and flow rate of the rectangular array design of ICEO micropump is performed in 3D and uses the Reciprocal Theorem,

$$\int \hat{\mathbf{u}} \cdot \mathbf{T} \cdot \hat{\mathbf{n}} dS = \int \mathbf{u} \cdot \hat{\mathbf{T}} \cdot \hat{\mathbf{n}} dS, \tag{1}$$

where $\mathbf{u}$ and $\mathbf{T}$ are the ICEO driven flow and $\hat{\mathbf{u}}$ and $\hat{\mathbf{T}}$ are Poiseuille flow in a rectangular channel [3],

$$\hat{\mathbf{u}}_y(x,z) = \frac{4s^2}{\pi^3 \eta} \frac{\partial \hat{P}}{\partial y} \sum_{n,odd}^{\infty} \frac{1}{n^3} \left(1 - \frac{\cosh \frac{n\pi z}{s}}{\cosh \frac{n\pi h}{2s}} \right) \sin \frac{n\pi x}{s}. \tag{2}$$

We assume fully developed Poiseuille flow in the channel running parallel to the longer rectangle axis. This assumption is valid for long pillars ($l \gg w$), but introduces an error otherwise. However, an extremely accurate expression is unnecessary for our purposes, which is simply to obtain an approximate design expression.

Figure 1 shows the geometry of the unit cell. While this unit cell could actually be broken down even further into four separate cells, we chose this unit cell because it allows a more intuitive derivation. First, the boundary conditions must be defined. In Figure 1, each of the surfaces in the unit cell cross-section have been labeled, while 'floor' and 'ceiling' (not shown) represent the bottom and top of the channel. The conditions on the micropillar surface, floor, and ceiling are listed first:

$$\hat{\mathbf{u}}_{no-slip} = \hat{\mathbf{u}}_{slip} = \hat{\mathbf{u}}_{floor} = \hat{\mathbf{u}}_{ceiling} = \mathbf{u}_{no-slip} = \mathbf{u}_{floor} = \mathbf{u}_{ceiling} = \mathbf{0} \tag{3}$$

$$\mathbf{u}_{slip} = \mathbf{u}_s \tag{4}$$

The analysis assumes a thin double layer ($\lambda_D \ll s$), allowing $\mathbf{u}_s$ to be modeled as a slip velocity. The Helmholtz-Smoluchowski velocity is often used, but slip velocity will vary greatly depending on experimental conditions, so we first solve the problem for a generic slip velocity.

The symmetry conditions along 'top' and 'bot' allow further simplification,

$$\mathbf{u}_{top} = \mathbf{u}_{bot} = (u_x, 0, 0); \tag{5}$$

$$\hat{\mathbf{u}}_{top} = \hat{\mathbf{u}}_{bot} = (\hat{u}_x, 0, 0); \tag{6}$$

$$T_{bot,xy} = T_{top,xy} = \hat{T}_{bot,xy} = \hat{T}_{top,xy} = 0; \tag{7}$$

$$\hat{\mathbf{n}}_{bot} = (0, 1, 0) = -\hat{\mathbf{n}}_{top}; \tag{8}$$

Taking the dot product of all the vectors results in zero contribution from the 'top' and 'bot' surfaces. Equation 1 has now been reduced to the following:

$$\int_{left,right} \hat{\mathbf{u}} \cdot \mathbf{T} \cdot \hat{\mathbf{n}} dA = \int_{left,right} \mathbf{u} \cdot \hat{\mathbf{T}} \cdot \hat{\mathbf{n}} dA + \int_{slip} \mathbf{u}_s \cdot \hat{\mathbf{T}} \cdot \hat{\mathbf{n}} dA \tag{9}$$

Simplifying the LHS by taking the dot product of the normal,

$$\int_{left} \hat{\mathbf{u}} \cdot \mathbf{T} \cdot \hat{\mathbf{n}} dA + \int_{right} \hat{\mathbf{u}} \cdot \mathbf{T} \cdot \hat{\mathbf{n}} dA = \int_{left} (\hat{u}_x T_{xx} + \hat{u}_y T_{yx} + \hat{u}_z T_{zx}) dA - \int_{right} (\hat{u}_x T_{xx} + \hat{u}_y T_{yx} + \hat{u}_z T_{zx}) dA \tag{10}$$

Both velocity profiles are the same is the same on the left and right side. For this reason, the stress tensors are also identical, except for the pressure term, resulting in.

$$\int_{left} \hat{\mathbf{u}} \cdot \mathbf{T} \cdot \hat{\mathbf{n}} dA + \int_{right} \hat{\mathbf{u}} \cdot \mathbf{T} \cdot \hat{\mathbf{n}} dA = \int_{right} \hat{u}_x P dA - \int_{left} \hat{u}_x P dA. \tag{11}$$

The pressure at these locations is not a strong function of y, so we assume it is constant in y, allowing a solution for the LHS

$$\int_{left,right} \hat{\mathbf{u}} \cdot \mathbf{T} \cdot \hat{\mathbf{n}} dA = \hat{Q} \Delta P \tag{12}$$

where $\Delta P = P_{right} - P_{left}$. Repeating this procedure for the second remaining integral results in

$$\int_{left,right} \mathbf{u} \cdot \hat{\mathbf{T}} \cdot \hat{\mathbf{n}} dA = Q \Delta \hat{P} \tag{13}$$

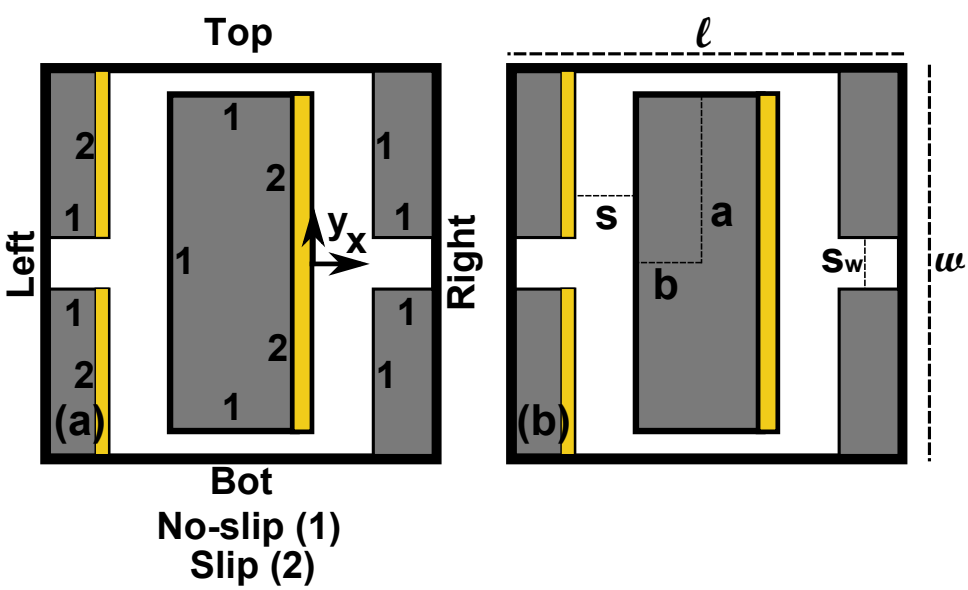

FIG. 1: (a) Boundary conditions for Reciprocal Theorem calculation. (b) Geometric parameter definitions.

Equation 1 has now become

$$\hat{Q}\Delta P - Q\Delta\hat{P} = 4\int_{slip} \mathbf{u}_s \cdot \hat{\mathbf{T}} \cdot \hat{\mathbf{n}} dA \tag{14}$$

where we noted that the four slipping surfaces provide the same contribution. Noting that $\mathbf{u}_s$=(0,u_s,0) allows further simplification.

$$\hat{Q}\Delta P - Q\Delta\hat{P} = 4\int_{slip} \eta u_s \frac{\partial \hat{u}_y}{\partial x} dydz \tag{15}$$

The hatted velocity is specified by Poiseuille flow, so that

$$\left.\frac{\partial \hat{u}_y}{\partial x}\right|_{x=wall} = \frac{4s}{\pi^2\eta}\frac{\partial \hat{P}}{\partial y}\sum_{n,odd}^{\infty}\frac{1}{n^2}\left(1 - \frac{\cosh\frac{n\pi z}{s}}{\cosh\frac{n\pi h}{2s}}\right) \tag{16}$$

We can now integrate out the z-dependence,

$$\begin{aligned}
\hat{Q}\Delta P - Q\Delta\hat{P} = 4\int_{slip} \eta u_s \frac{\partial \hat{u}_y}{\partial x} dydz \\
&= \frac{16s}{\pi^2}\frac{\partial \hat{P}}{\partial y}\int_{slip} u_s(y)\sum_{n,odd}^{\infty}\frac{1}{n^2}\left(1 - \frac{\cosh\frac{n\pi z}{s}}{\cosh\frac{n\pi h}{2s}}\right) dydz \\
&= \frac{16s^2}{\pi^2}\frac{\partial \hat{P}}{\partial y}\left(\int_{slip} u_s(y)dy\right)\sum_{n,odd}^{\infty}\frac{h}{sn^2}\left(1 - \frac{2s\tanh\frac{n\pi h}{2s}}{hn\pi}\right) \\
&= \frac{16s^2}{\pi^2}\frac{\partial \hat{P}}{\partial y} f(A)\int_{slip} u_s(y)dy
\end{aligned} \tag{17}$$

where $A = h/s$ is the gap aspect ratio and $f(A)$ is the entire summation (for A=1, f(A)= 0.617). The Poiseuille flow splits down the two halfs of the unit cell so that the pressure gradient along each slipping surface is half the total drop across the cell, $\frac{\partial \hat{P}}{\partial y} \approx \frac{-\Delta\hat{P}}{2(2a+4b+2s+s_w)} = \frac{-\Delta\hat{P}}{p}$ with unit cell perimeter p. Q_{max} for a cell is Q when ΔP=0, resulting in

$$Q_{max} = \frac{16s^2}{p\pi^2} f(A)\int_{slip} u_s(y)dy \tag{18}$$

Likewise, the cell ΔP_{max} is given when $Q = 0$. $\hat{Q}$ is the pressure driven flow rate through the entire cell, which is twice the flow rate through an individual channel along a slipping surface,

$$\hat{Q} = \frac{16s^4}{\pi^4\eta}\frac{\partial \hat{P}}{\partial y}\sum_{n,odd}^{\infty}\frac{h}{sn^4}\left(1 - \frac{2s}{n\pi h}\tanh\frac{n\pi h}{2s}\right), \tag{19}$$

the maximum pressure for a cell is

$$\Delta P_{max} = \frac{\pi^2\eta}{s^2}\frac{f(A)}{g(A)}\int_{slip} u_s(y)dy \tag{20}$$

where g(A) is summation shown in $\hat{Q}$ (for A=1, g(A)=0.428, and f(A)/g(A)=1.44).

The total pump flow rate and pressure drop can be found for an NxM array of unit cells with total length L and total width W.

$$N = \frac{L}{l} = \frac{L}{4b + 2s} \tag{21}$$

$$M = \frac{W}{w} = \frac{W}{2a + s_w} \tag{22}$$

The maximum total flow rate is

$$Q_{max} = MQ_{cell} \tag{23}$$
$$= \frac{W}{2a+s_w}\frac{16s^2}{p\pi^2}f(A)\int_{slip} u_s(y)dy.$$

The maximum total pressure is

$$\Delta P_{max} = N\Delta P_{cell}$$
$$= \frac{L}{l}\frac{\pi^2\eta}{s^2}\frac{f(A)}{g(A)}\int_{slip} u_s(y)dy. \tag{24}$$

To simplify, we limit several values to those used for the fabrication method presented here. In particular, we set $A = 1$, $s = 2b$, $4s = l$, and $2.5s_w = a$. This results in a maximum pressure and flow rate

$$\boxed{\Delta P_{max} = 3.6\frac{L\eta}{s^3}\int_{slip} u_s(y)dy} \tag{25}$$

$$\boxed{Q_{max} = 0.21\frac{W}{a}\frac{s^2}{(a+2s)}\int_{slip} u_s(y)dy} \tag{26}$$

The above equations could be combined with numerical computation of slip velocity depending on the physics one wants to incorporate, however this goes beyond the scope of our work. We simply seek a scaling expression, so we insert the Helmholtz-Smoluchowski velocity for time-averaged ICEO flow in the low frequency, low-ζ limit with correction factor Λ,

$$u_s = \frac{\epsilon E\zeta_i(y)}{2\eta} = \frac{\Lambda\epsilon E^2 y}{2\eta}. \tag{27}$$

In this case, the equations become

$$\Delta P_{max} = 0.9\frac{\Lambda\epsilon La^2E^2}{s^3} = 0.9\frac{\Lambda\epsilon La^2\phi^2}{W^2s^3} \tag{28}$$

$$Q_{max} = 0.05\frac{\Lambda\epsilon Was^2E^2}{\eta(a+2s)} = 0.05\frac{\Lambda\epsilon as^2\phi^2}{W\eta(a+2s)} \tag{29}$$

where ϕ is the amplitude of the applied voltage.

[1] Vincent Studer, Giao Hang, Anna Pandolfi, Michael Ortiz, W. French Anderson, and Stephen R. Quake. Scaling properties of a low-actuation pressure microfluidic valve. *Journal of applied physics*, 95(1):393398, 2004.

[2] Andrew J. Pascall. *Ph.D. Thesis.* 2010.

[3] H. Bruus. *Theoretical microfluidics*, volume 18. Oxford University Press, USA, 2007.